

LLM-DRIVEN SCENARIO-AWARE PLANNING FOR AUTONOMOUS DRIVING

He Li¹, Zhaowei Chen¹, Rui Gao³, Guoliang Li¹, Qi Hao³, Shuai Wang^{2,†}, and Chengzhong Xu^{1,†}

¹University of Macau ²Shenzhen Institutes of Advanced Technology, Chinese Academy of Sciences

³Southern University of Science and Technology

ABSTRACT

Hybrid planner switching framework (HPSF) for autonomous driving needs to reconcile high-speed driving efficiency with safe maneuvering in dense traffic. Existing HPSF methods often fail to make reliable mode transitions or sustain efficient driving in congested environments, owing to heuristic scene recognition and low-frequency control updates. To address the limitation, this paper proposes LAP, a large language model (LLM) driven, adaptive planning method, which switches between high-speed driving in low-complexity scenes and precise driving in high-complexity scenes, enabling high qualities of trajectory generation through confined gaps. This is achieved by leveraging LLM for scene understanding and integrating its inference into the joint optimization of mode configuration and motion planning. The joint optimization is solved using tree-search model predictive control and alternating minimization. We implement LAP by Python in Robot Operating System (ROS). High-fidelity simulation results show that the proposed LAP outperforms other benchmarks in terms of both driving time and success rate.

Index Terms— Scenario-aware, autonomous driving, large language model

1. INTRODUCTION

How to drive efficiently under various driving scenarios, e.g., dense traffic, highway driving, is the crucial issue for autonomous driving (AD) [1, 2]. Conventional AD methods struggle with adaptability: some universally apply strict collision avoidance, which is overly conservative in many contexts [3, 4], while others are designed for high-speed driving but assume static or obstacle-free environments [5, 6]. To address this issue, a promising solution is a hybrid planner switching framework (HPSF), which can flexibly adapt to multiple driving modes instead of a single scenario.

The main challenge to realizing HPSF is determining the appropriate timing for switching between driving modes.

This work was supported by the National Key R&D Program of China (No. 2025YFE0204100), Science and Technology Development Fund of Macao S.A.R (FDCT) under number 0074/2025/AMJ, the National Natural Science Foundation of China (Grant No. 62371444), and the Shenzhen Science and Technology Program (Grant No. RCYX20231211090206005, JCYJ20241202124934046). Corresponding author: Chengzhong Xu (czxu@um.edu.mo) and Shuai Wang (s.wang@siat.ac.cn)

First, switching to an inappropriate mode may compromise driving efficiency or even safety. For example, engaging dense-traffic mode on highways reduces speed, while activating high-speed mode in congested traffic increases collision risk. Second, efficient driving in dense traffic remains challenging. Existing HPSF approaches struggle to align driving styles with scene demands due to reliance on simple heuristic scene-recognition methods [7, 8]. Moreover, low operating frequency (< 20Hz) in dense traffic [3, 9] further restricts performance across diverse scenarios.

To fill this gap, this paper proposes an **LLM**-driven **Adaptive Planner**, termed as LAP. The LAP method integrates an LLM-driven mode switcher, which can infer the appropriate driving strategy in real time like a human driver with a driving knowledge database and scenario description. Guided by the LLM, the system dynamically selects between two complementary modes: a fast driving (FD) mode that adopts active maneuvers to push the vehicle to its dynamic limit in regions with sparsely distributed obstacles, and a shape-aware (SA) mode that carefully navigates in regions with densely distributed obstacles. Combining situation awareness with context-dependent planning enables robust real-time performance in diverse scenarios. Technically, we determine when to engage FD or SA by solving an LLM-guided joint optimization of style configuration and motion planning. The optimization is carried out using tree-search model predictive control (TMPC) and alternating minimization (AM). We implement the LAP in Python as a Robot Operating System (ROS) package and verify its performance on the Carla simulation platform. Results show that LAP effectively adapts to diverse scenarios, achieving a higher driving speed and more reliable overtaking performance than other benchmarks.

2. PROBLEM FORMULATION

We consider the driving scenario shown on the left-hand side of Fig. 1. We adopt the MPC formulation for HPSF, where the future states are predicted via robot dynamics over an H -step receding horizon. It optimizes vehicle states $\{\mathbf{s}_t, \dots, \mathbf{s}_{t+H-1}\}$ ($\mathbf{s}_t = [x_t, y_t, \theta_t]^T$ with position (x_t, y_t) and orientation θ_t) and actions $\{\mathbf{u}_t, \dots, \mathbf{u}_{t+H-1}\}$ ($\mathbf{u}_t = [v_t, \psi_t]^T$ with linear velocity v_t and angular velocity ψ_t) under state evolution and action boundary constraints.

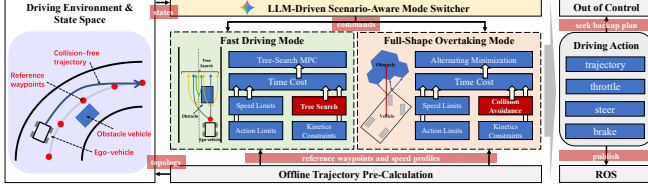


Fig. 1: System architecture of LAP.

First, the state evolution is given by $\mathbf{s}_{t+1} = E(\mathbf{s}_t, \mathbf{u}_t)$, where

$$E(\mathbf{s}_t, \mathbf{u}_t) = \mathbf{A}_t \mathbf{s}_t + \mathbf{B}_t \mathbf{u}_t + \mathbf{c}_t, \quad \forall t, \quad (1)$$

and $(\mathbf{A}_t, \mathbf{B}_t, \mathbf{c}_t)$ are coefficient matrices of Ackermann kinetics defined in equations (8)–(10) of [10, Sec. III-B]. Using (1), we can compute state $\mathbf{s}_{t+h+1} = E(\mathbf{s}_{t+h}, \mathbf{u}_{t+h})$ for any $h \in [0, H-1]$. Second, the driving action is bounded by

$$\begin{aligned} \mathbf{u}_{\min} \preceq \mathbf{u}_{t+h} \preceq \mathbf{u}_{\max}, \quad \forall h, \\ \mathbf{a}_{\min} \preceq \mathbf{u}_{t+h+1} - \mathbf{u}_{t+h} \preceq \mathbf{a}_{\max}, \quad \forall h, \end{aligned} \quad (2)$$

where \mathbf{u}_{\min} and \mathbf{u}_{\max} are the minimum and maximum values of the control vector, respectively, and \mathbf{a}_{\min} and \mathbf{a}_{\max} are the associated minimum and maximum acceleration bounds. The entire physical constraints are thus $\{\mathbf{s}_{t+h}, \mathbf{u}_{t+h}\} \in \mathcal{P}$ with $\mathcal{P} = \{\{\mathbf{s}_{t+h}, \mathbf{u}_{t+h}\} : (1), (2)\}$. Given the pre-calculated pose \mathbf{s}_t^\diamond and speed v_t^\diamond (detailed in Section III-A), the HPSF problem P0 is [3]:

$$\begin{aligned} \text{P0: } \min_{\{\mathbf{s}_{t+h}, \mathbf{u}_{t+h}\} \in \mathcal{P}} \sum_{h=0}^H & \underbrace{\left(\|\mathbf{s}_{t+h} - \mathbf{s}_{t+h}^\diamond\|^2 + \|v_{t+h} - v_{t+h}^\diamond\|^2 \right)}_{:=C_0\left(\{\mathbf{s}_{t+h}, \mathbf{u}_{t+h}\}_{h=0}^H\right)} \\ & (3a) \end{aligned}$$

$$\text{s.t. } \mathbf{dist}(\mathbf{s}_{t+h}, \mathbf{o}_{i,t+h}) \geq d_{\text{safe}}, \quad \forall i, h, \quad (3b)$$

where (3b) is the collision avoidance constraint, $\mathbf{dist}(\mathbf{s}_t, \mathbf{o}_{i,t})$ is the distance between the ego-vehicle and the i -th obstacle at time t , and d_{safe} in meter is a pre-defined safety distance.

Solving problem P0 is nontrivial due to the bilevel collision-avoidance constraint (3b). Embedding this constraint directly in the optimizer would compromise frequency, whereas approximating $\{\mathbf{o}_{i,t+h}\}$ into sets [3] or voxels [11] would compromise accuracy. Below, we present an effective LLM solution to tackle this challenge.

3. LLM DRIVEN ADAPTIVE PLANNING

3.1. System Overview

The architecture of LAP is shown in Fig. 1, which reads the topology and states including poses of ego- and other-vehicles (on the left hand side of Fig. 1) from the driving route and vehicle sensors, and outputs collision-free trajectories and associated driving actions including steer, throttle, and brake (on the right hand side of Fig. 1).

The pipeline starts with offline pre-computation. The circuit is segmented into geometric primitives (straights/curves), and an optimization kernel pre-generates high-resolution, vehicle-dynamics-aware driving waypoints $\{\mathbf{s}_t^\diamond\}$ and speed envelopes $\{v_t^\diamond\}$ using an offline pure pursuit (PP) algorithm. Note that the actual path may differ from the pre-calculated one due to dynamic obstacle avoidance.

During the online planning phase, the snapshot is fed to a scenario-aware planner switcher powered by an LLM. The switcher issues a command vector $\mathbf{c} = \{c_1, c_2\}$, where $c_1 \in \{fd, sa\}$ selects either the FD mode for aggressive behavior or the SA mode for conservative driving, and $c_2 \in \{acc, keep, dec\}$ recommends a speed for acceleration or deceleration. To translate text vector \mathbf{c} into executable commands, we introduce mapping $\mathcal{M}_1 : c_1 \rightarrow \beta$ with $\beta \in \{0, 1\}$, where $\beta = 0$ selects FD mode, while $\beta = 1$ selects SA mode. To translate the speed reference vector, we introduce mapping $\mathcal{M}_2 : c_2 \rightarrow \gamma$, such that $\gamma \in \{v_0, 0, -v_0\}$, corresponding to $\{acc, keep, dec\}$, respectively, where v_0 is the pre-defined velocity shift.

3.2. LAP Cost and Constraints

The cost function of LAP is based on (3a) but needs to incorporate the LLM inference γ for adaptive planning. Given the original reference speed v_t^\diamond , the updated reference speed is $v_t^\diamond \leftarrow v_t^\diamond + \gamma$. Then the cost function becomes

$$\begin{aligned} C_1(\{\mathbf{s}_{t+h}, \mathbf{u}_{t+h}\}_{h=0}^H) = \sum_{h=0}^H & \left(\|\mathbf{s}_{t+h} - \mathbf{s}_{t+h}^\diamond\|^2 \right. \\ & \left. + \|v_{t+h} - v_{t+h}^\diamond - \gamma\|^2 \right), \quad (4) \end{aligned}$$

On the other hand, LAP builds on (3b) and incorporates the mode β to balance computational speed and obstacle-avoidance accuracy. If $\beta = 0$ (FD mode), we sample M paths on the route, where the waypoints of the m -th path are $\mathcal{W}_m = \{\mathbf{w}_{m,1}, \mathbf{w}_{m,2}, \dots\}$. Then optimizing $\{\mathbf{s}_{t+h}\}$ is transformed into optimizing path selection α_m (with $\alpha_m \in \{0, 1\}$ and $\sum_m \alpha_m = 1$), and (3b) is reformulated as

$$\begin{aligned} (1 - \beta) \left\| \mathbf{s}_{t+h} - \sum_{m=1}^M \alpha_m \mathbf{w}_{m,t+h} \right\| & \leq \epsilon, \quad \forall h, \\ (1 - \beta) \left[\mathbf{dist} \left(\sum_{m=1}^M \alpha_m \mathbf{w}_{m,t+h}, \mathbf{o}_{i,t+h} \right) - d_{\text{safe}} \right] & \geq 0, \quad \forall i, h, \quad (5) \end{aligned}$$

where $\epsilon > 0$ is a small deviation constant.

If $\beta = 1$ (SA mode), the LAP will consider the full shape of objects. Accordingly, the minimum distance in (3b) be-

tween full-shape ego-vehicle and obstacle vehicle is given by

$$\text{dist}(\mathbf{s}_t, \mathbf{o}_{i,t}) = \min \{ \|\mathbf{e}\|_2 \mid (\mathbb{Z}_t(\mathbf{s}_t) + \mathbf{e}) \cap \mathbb{O}(\mathbf{o}_{i,t}) \neq \emptyset \}, \quad (6)$$

$\mathbb{Z}_t(\mathbf{s}_t)$ and $\mathbb{O}(\mathbf{o}_{i,t})$ are the compact convex sets occupied by the ego and i -th obstacle vehicles, which can be represented by the conic inequality [12]:

$$\begin{aligned} \mathbb{O}_{i,t} &= \{\mathbf{o} \mid \mathbf{D}_{i,t} \mathbf{o} \preceq \mathbf{b}_{i,t}\}, \\ \mathbb{Z}_t(\mathbf{s}_t) &= \mathbf{R}_t(\mathbf{s}_t) \mathbf{z} + \mathbf{p}_t(\mathbf{s}_t), \forall \mathbf{z} \in \mathbb{C}, \\ \mathbb{C} &= \{\mathbf{z} \mid \mathbf{G} \mathbf{z} \preceq \mathbf{h}\}, \end{aligned} \quad (7)$$

where, $[\mathbf{D}_{i,t}, \mathbf{b}_{i,t}]$ and $[\mathbf{G}, \mathbf{h}]$ are decided by the shape of i -th obstacle vehicle and ego-vehicle respectively. $\mathbf{p}_t(\mathbf{s}_t)$ and $\mathbf{R}_t(\mathbf{s}_t)$ are the transition and rotation matrices.

The set computation in (6) is non-convex and non-differential. To resolve this challenge, we adopt the strong duality to transform constraint (6) into a more computationally efficient form [3, 10], and then constraint (3b) becomes

$$\begin{aligned} \beta \begin{bmatrix} -\boldsymbol{\lambda}_{i,t} \\ -\boldsymbol{\mu}_{i,t} \\ d_{\text{safe}} - \boldsymbol{\lambda}_{i,t}^\top \mathbf{D}_{i,t} \mathbf{p}_t(\mathbf{s}_t) + \boldsymbol{\lambda}_{i,t}^\top \mathbf{b}_{i,t} + \boldsymbol{\mu}_{i,t}^\top \mathbf{h} \\ \|\mathbf{D}_{i,t}^\top \boldsymbol{\lambda}_{i,t}\|_* - 1 \end{bmatrix} &\leq \mathbf{0}, \quad (8) \\ \beta [\boldsymbol{\mu}_{i,t}^\top \mathbf{G} + \boldsymbol{\lambda}_{i,t}^\top \mathbf{D}_{i,t} \mathbf{R}_t(\mathbf{s}_t)] &= \mathbf{0}, \end{aligned}$$

where, $\boldsymbol{\lambda}_{i,t}$ and $\boldsymbol{\mu}_{i,t}$ are the dual variables.

3.3. LLM-Driven LAP Algorithm Design

Based on the analysis in 3.2, we write the problem P0 as

$$\begin{aligned} \text{P1 : } \min_{\{\alpha_m, \beta, \gamma\}, \{\mathbf{s}_{t+h}, \mathbf{u}_{t+h}\}, \{\boldsymbol{\lambda}_{i,t+h}, \boldsymbol{\mu}_{i,t+h}\}} \quad &C_2(\{\mathbf{s}_{t+h}, \mathbf{u}_{t+h}\}_{h=0}^H) \\ \text{s.t. constraints (1), (2), (5), (8)} \end{aligned} \quad (9)$$

$$\alpha_m, \beta \in \{0, 1\}, \gamma \in \{-v_0, 0, v_0\}, \sum_{m=1}^M \alpha_m = 1. \quad (10)$$

It can be seen that P1 involves joint optimization of mode configuration and motion planning.

Conventional methods utilize a rule-based planner switcher with rules to select $\{\alpha_m, \beta, \gamma\}$. However, pre-defined rules are difficult to generalize across diverse scenarios. To address this, we introduce an LLM-based switcher \mathcal{L} (*LLM-switcher*) that selects the appropriate driving mode. At each timestep t , the LLM receives as input the system state \mathbf{s}_t and environmental context \mathbf{p}_t . Following the retrieval-augmented generation (RAG) [13] method, we create a database \mathcal{U} with the retrieval mechanism Q , where \mathcal{U} contains driving experience, including strategies that can be adopted when dealing with situations, and Q uses $\mathbf{s}_t, \mathbf{p}_t$ to retrieve top k historical experience $Q(\mathbf{s}_t, \mathbf{p}_t, \mathcal{U}) \rightarrow \{q_{t,1}, q_{t,2}, \dots, q_{t,k}\}$, that is used

as reference control policy. Then the LLM generates the high-level commands \mathbf{c} through chain-of-thought reasoning:

$$\mathcal{L}(\mathbf{s}_t, \mathbf{p}_t, \{q_{t,1}, q_{t,2}, \dots, q_{t,k}\}) \rightarrow \mathbf{c} = \{c_1, c_2\}. \quad (11)$$

We then obtain the solution of $\{\beta, \gamma\}$ to P1 as

$$\beta = \mathcal{M}_1(c_1), \gamma = \mathcal{M}_2(c_2). \quad (12)$$

With solution $\{\beta, \gamma\}$, we consider two cases. If $\beta = 0$ (FD mode), constraints (1), (2), (5) become active, and P1 is a mixed-integer nonlinear optimization problem. To solve it, we first determine the path samples $\{\mathbf{w}_{m,t+h}\}$ using MPC under constraints (1) and (2). This would generate M candidate solutions of $\{\mathbf{s}_{t+h}^{(m)}, \mathbf{u}_{t+h}^{(m)}\}$. Then we determine the optimal value of $\{\alpha_m\}$ and a tree search approach is adopted to explore all possible $\{\alpha_m\}$. For each fixed $\{\alpha_m\}$ we check if $\Theta(\{\alpha_m\}) \geq d_{\text{safe}}$ holds. If so, we add this solution to the candidate set $\mathcal{F} = \mathcal{F} \cup \{\alpha_1, \alpha_2, \dots\}$; otherwise this trail is abandoned. The optimal $\{\alpha_1^*, \alpha_2^*, \dots\}$ is selected from \mathcal{F} by minimizing the deviation between the $\{\mathbf{s}_{t+h}^{(m)}\}$ and the target waypoints $\{\mathbf{s}_{t+h}^*\}$. The optimal motion is $\{\mathbf{s}_{t+h}^* = \sum_m \alpha_m^* \mathbf{s}_{t+h}^{(m)}, \mathbf{u}_{t+h}^* = \sum_m \alpha_m^* \mathbf{u}_{t+h}^{(m)}\}$.

If $\beta = 1$ (SA mode), constraints (1), (2), and (8) become active. This problem no longer involves integers $\{\alpha_m\}$ but is non-convex because of the coupled variables $\{\mathbf{s}_{t+h}, \mathbf{u}_{t+h}, \boldsymbol{\lambda}_{i,t+h}, \boldsymbol{\mu}_{i,t+h}\}$. Fortunately, the subproblem of $\{\mathbf{s}_{t+h}, \mathbf{u}_{t+h}\}$ is convex with given fixed $\{\boldsymbol{\lambda}_{i,t+h}, \boldsymbol{\mu}_{i,t+h}\}$; and vice versa. To this end, the SA mode leverages the AM framework to solve this optimization problem in an alternative way. The idea is to split the variables into two groups, $\{\mathbf{s}_{t+h}, \mathbf{u}_{t+h}\}$ and $\{\boldsymbol{\lambda}_{i,t+h}, \boldsymbol{\mu}_{i,t+h}\}$, and then update each group of variables with the other fixed. Each subproblem is efficiently solved by off-the-shelf software, e.g., cvxpy [14]. The AM procedure starts with an initial solution from the previous frame and terminates after 2 to 3 iterations. This completes a LAP iteration and we update $t \leftarrow t + 1$. The LLM-switcher is periodically triggered at 1 Hz and reactively triggered upon obstacle detection. This trigger mechanism enables both continuous adaptation and safety-critical responses. Note that motion control executes at up to 100 Hz.

4. EXPERIMENTS

We implemented the proposed LAP system using Python in ROS. The high-fidelity MetaGrandPrix simulation platform is used for evaluations, which is 1:1 constructed according to the real-world Macau Grand Prix circuit in the CARLA [15] simulator, available here. Our LAP system is connected to MetaGrandPrix via ROS bridge [16]. All simulations are implemented on a Ubuntu workstation with an Intel Core i9-11900 CPU and an NVIDIA 4090 GPU.

First, we evaluate the LLM-switcher across multiple models. We evaluate GPT-4o-mini [17], Qwen3-32B [18], Gemini-2.0-Flash [19], and Llama-3.3-70B [20] as candidate LLMs. Given the real-time demands of driving, latency must

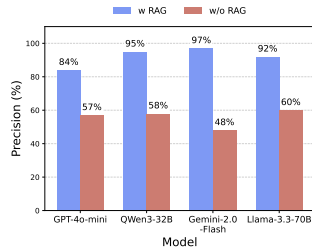


Fig. 2: Evaluation of LLMs.

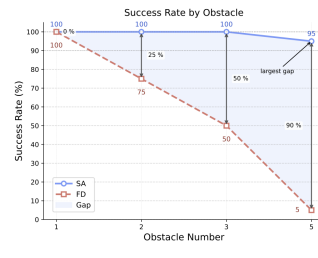


Fig. 3: Overtaking results.

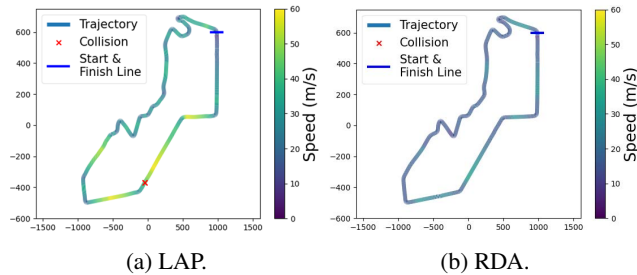


Fig. 4: Racing trajectories.

be balanced with reasoning capability. As shown in Fig. 5, the average Time To First Token (TTFT) across all models is under 0.5 s, indicating suitability for the LAP. Specifically, we test candidate LLMs against an expert dataset comprising hundreds of samples, measuring precision as the match rate with expert outputs. The results in Fig. 2 show that RAG markedly improves the precision of all four LLMs in the scenario-aware switcher, with gains of at least 27%. Gemini-2.0-Flash demonstrates the largest improvement, rising from 48% without RAG to 97% with RAG. Among RAG-enhanced models, Gemini-2.0-Flash outperforms GPT-4o-mini (84%), Qwen3-32B (95%), and Llama-3.3-70B (92%). Therefore, we utilize Gemini-2.0-Flash with RAG as the mode switcher in the following experiments.

Next, we evaluate the driving capability of FD and SA modes under progressively denser traffic. They are required to perform overtaking maneuvers with background vehicle density increases from one to five obstacles. Each mode was executed 20 times for each density level. Success rates are reported in Fig. 3. LAP achieves 100% success in the sparsest setting under both modes. As density increases, FD mode performance degrades sharply—75% with two opponents, 50% with three, and only 5% with five. In contrast, SA mode remains robust, sustaining 100% up to three opponents and 95% at maximum density. These results show that FD mode suffices in light traffic, but the SA mode provides superior robustness in dense scenarios. The gap arises because FD models rivals as point centers and uses a coarse lane-based tree that collapses in congestion, whereas SA considers full vehicle geometry and preserves feasible corridors for overtaking. This confirms the necessity of SA for high-density scenarios.

Finally, we evaluate LAP in a high-speed scenario, measuring the best lap time over 10 trials. The track contains 10 sparsely distributed background vehicles controlled by a

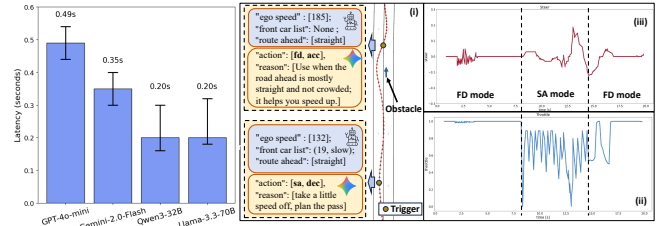


Fig. 5: TTFT. Fig. 6: Illustration of LAP in CARLA.

Table 1: Comparison of different racing approaches

Method	lap time (s)	avg. speed (km/h)	colli. num [†]	max speed (km/h)
CF-based PP	932.70	25.09	12	51.05
RDA [10]	526.35	44.46	0	112.68
FSM Speed [21]*	271.30	86.25	1	—
Optimistic (Ours)	265.65	88.09	1	211.31
LAP (Ours)	269.13	86.95	1	211.20

* Champion of the 2023 Grand Prix Metaverse AD Challenge.

† Racing allows collision as long as the vehicle can proceed.

conventional MPC-based planner. LAP is compared against the following benchmarks: 1) **CF-based PP**: CARLA’s built-in planner that follows the lead vehicle and accelerates when the lane is clear; 2) **RDA planner**: An accelerated full-shape MPC planner solving P1 in parallel via ADMM [10]; 3) **Optimistic**: LAP without obstacles. An illustration of LAP is shown in Fig. 6, and the quantitative results are presented in Table. 1. The CF-based PP requires 932.7 s to complete the race (25 km/h average) due to its passive collision-avoidance strategy and poor lateral control. The shape-aware RDA planner halves the lap time to 526 s and eliminates collisions, but its operation frequency (i.e., 20 Hz) limits the peak speed at 113 km/h (as illustrated in Fig. 4b). In contrast, the proposed LAP finishes in 269.13 s, with an average speed of 86.9 km/h and peak velocity of 211 km/h. The racing trajectory of LAP in Fig. 4a also corroborates the performance. This performance is close to the optimistic upper bound under no obstacles, which is 265.65 s with a peak speed of 211 km/h. Notably, the proposed LAP even outperforms the champion in the competition (271.3 s) [21]. This result shows that the LLM-driven scenario-aware mode switcher can efficiently select the proper planner mode, and achieve the optimal balance between precise overtaking and fast driving.

5. CONCLUSION

This paper presented LAP, an HPSF method designed for dynamic driving scenarios. Experiments demonstrated that LAP balances the speed performance and safety assurance in dense traffic. In the high-speed setting, LAP switched between TMPC-based FD and AM-based SA, with TMPC driving the vehicle near its limits and AM enabling accurate overtaking. The vehicle with LAP was able to reach speeds of up to 211 km/h and achieve a lap time close to the optimistic scheme (< 5 s gap).

6. REFERENCES

[1] Jingyuan Zhao, Yuyan Wu, Rui Deng, Susu Xu, Jinpeng Gao, and Andrew Burke, “A survey of autonomous driving from a deep learning perspective,” *ACM Computing Surveys*, vol. 57, no. 10, pp. 1–60, 2025.

[2] David González, Joshué Pérez, Vicente Milanés, and Fawzi Nashashibi, “A review of motion planning techniques for automated vehicles,” vol. 17, no. 4, pp. 1135–1145, 2015.

[3] Xiaojing Zhang, Alexander Liniger, and Francesco Borrelli, “Optimization-based collision avoidance,” *IEEE Transactions on Control Systems Technology*, vol. 29, no. 3, pp. 972–983, 2020.

[4] Christoph Rösmann, Frank Hoffmann, and Torsten Bertram, “Kinodynamic trajectory optimization and control for car-like robots,” in *2017 IEEE/RSJ International Conference on Intelligent Robots and Systems (IROS)*. IEEE, 2017, pp. 5681–5686.

[5] Jonathan Becker, Nadine Imholz, Luca Schwarzenbach, Edoardo Ghignone, Nicolas Baumann, and Michele Magno, “Model-and acceleration-based pursuit controller for high-performance autonomous racing,” in *2023 IEEE International Conference on Robotics and Automation (ICRA)*. IEEE, 2023, pp. 5276–5283.

[6] Aliasghar Arab, Kaiyan Yu, Jiaxing Yu, and Jingang Yi, “Motion planning and control of autonomous aggressive vehicle maneuvers,” *IEEE Transactions on Automation Science and Engineering*, 2023.

[7] Tim Stahl, Alexander Wischnewski, Johannes Betz, and Markus Lienkamp, “Multilayer graph-based trajectory planning for race vehicles in dynamic scenarios,” in *2019 IEEE Intelligent Transportation Systems Conference (ITSC)*. IEEE, 2019, pp. 3149–3154.

[8] Mingyu Wang, Zijian Wang, John Talbot, J Christian Gerdes, and Mac Schwager, “Game-theoretic planning for self-driving cars in multivehicle competitive scenarios,” *IEEE Transactions on Robotics*, vol. 37, no. 4, pp. 1313–1325, 2021.

[9] Zeqing Zhang, Yinqiang Zhang, Ruihua Han, Liangjun Zhang, and Jia Pan, “A generalized continuous collision detection framework of polynomial trajectory for mobile robots in cluttered environments,” *IEEE Robotics and Automation Letters*, vol. 7, no. 4, pp. 9810–9817, 2022.

[10] Ruihua Han, Shuai Wang, Shuaijun Wang, Zeqing Zhang, Qianru Zhang, Yonina C Eldar, Qi Hao, and Jia Pan, “Rda: An accelerated collision free motion planner for autonomous navigation in cluttered environments,” *IEEE Robotics and Automation Letters*, vol. 8, no. 3, pp. 1715–1722, 2023.

[11] Ji Zhang, Chen Hu, Rushat Gupta Chadha, and Sanjiv Singh, “Falco: Fast likelihood-based collision avoidance with extension to human-guided navigation,” *Journal of Field Robotics*, vol. 37, no. 8, pp. 1300–1313, 2020.

[12] Stephen Boyd, Stephen P Boyd, and Lieven Vandenberghe, *Convex Optimization*, Cambridge university press, 2004.

[13] Patrick Lewis, Ethan Perez, Aleksandra Piktus, Fabio Petroni, Vladimir Karpukhin, Naman Goyal, Heinrich Küttler, Mike Lewis, Wen-tau Yih, Tim Rocktäschel, et al., “Retrieval-augmented generation for knowledge-intensive nlp tasks,” *Advances in Neural Information Processing Systems (NeurIPS)*, vol. 33, pp. 9459–9474, 2020.

[14] Steven Diamond and Stephen Boyd, “CVXPY: A Python-embedded modeling language for convex optimization,” *Journal of Machine Learning Research*, vol. 17, no. 83, pp. 1–5, 2016.

[15] Alexey Dosovitskiy, German Ros, Felipe Codevilla, Antonio Lopez, and Vladlen Koltun, “Carla: An open urban driving simulator,” in *Conference on Robot Learning*, 2017, vol. 78, pp. 1–16.

[16] Intel, “ROS/ROS2 bridge for CARLA simulator,” <https://github.com/carla-simulator/ros-bridge>, 2023.

[17] Aaron Hurst and 416 others, “Gpt-4o system card,” *arXiv preprint arXiv:2410.21276*, 2024.

[18] An Yang, Anfeng Li, Baosong Yang, Beichen Zhang, Binyuan Hui, Bo Zheng, Bowen Yu, Chang Gao, Chengan Huang, Chenxu Lv, et al., “Qwen3 technical report,” *arXiv preprint arXiv:2505.09388*, 2025.

[19] Gemini Team, Rohan Anil, Sebastian Borgeaud, Jean-Baptiste Alayrac, Jiahui Yu, Radu Soricut, Johan Schalkwyk, Andrew M Dai, Anja Hauth, Katie Millican, et al., “Gemini: a family of highly capable multimodal models,” *arXiv preprint arXiv:2312.11805*, 2023.

[20] Abhimanyu Dubey, Abhinav Jauhri, Abhinav Pandey, Abhishek Kadian, Ahmad Al-Dahle, Aiesha Letman, Akhil Mathur, Alan Schelten, Amy Yang, Angela Fan, et al., “The llama 3 herd of models,” *arXiv e-prints*, pp. arXiv–2407, 2024.

[21] “Grand prix metaverse autonomous driving challenge,” 2023, Available at: https://contests.cis.um.edu.mo/meta_racing_2023/.